Optoelectronic Properties of Natural Cyanin Dyes

A. Calzolari,*,† D. Varsano,†,# A. Ruini,†,‡ A. Catellani,§ R. Tel-Vered,|| H. B. Yildiz,|| O. Ovits,|| and I. Willner||

National Center on nanoStructures and bioSystems at Surfaces (S3) of CNR-INFM, Via Campi 213/A, 41100 Modena, Italy, Dipartimento di Fisica, Università di Modena e Reggio Emilia, Via Campi 213/A, 41100 Modena, Italy, CNR-IMEM, Parco Area delle Scienze, 37A, I-43100 Parma, Italy, and Institute of Chemistry, The Hebrew University of Jerusalem, Jerusalem 91904, Israel

Received: May 27, 2009

An integrated theoretical/experimental study of the natural cyanin dye is presented in terms of its structural and optoelectronic properties for different gas-phase and prototypical device configurations. Our microscopic analysis reveals the impact of hydration and hydroxylation reactions, as well as of the attached sugar, on ground and optically excited states, and it illustrates the visible-light harvesting capability of the dye. Our optical experiments at different and controlled pH concentrations allow for a direct comparison with theoretical results. We analyze the many different contributions to photocurrent of the various portions of a prototypical device and, as a proof of principle, we propose the addition of specific ligands to control the increase of the photocurrent yield in the cyanin-based electrochemical device.

1. Introduction

The flavonoid compounds are one of the most ubiquitous classes of natural products, especially interesting due to their peculiar interactions with light. They are commonly found in plants, where they act as protective agents in response to various environmental signals; they strongly absorb UV−vis radiation and their accumulation in leaf epidermis is strictly connected to their specific function against radiation damage. The optical activity of flavonoids is particularly engaging in the case of anthocyanins, which have been subject of study because of their fundamental role as natural dyes in vegetables,[1] being responsible for the red, blue, and purple colors of many flowers, plants and fruits. Their colorant properties[2] and their peculiar ability in absorbing UV radiation along with their large bioavailability and their low cost have been exploited in food industry and pharmaceutical preparations.[3−5] Anthocyanins also act as effective free radical scavengers and are able to chelate metal ions; thus, they exhibit antioxidant activity and they strongly reduce the metal-induced peroxidation in biosystems[6,7] and therefore are utilized as antiatherosclerosis and anticarcinogenic agents.[8] Recently, a completely different kind of application has been advanced for anthocyanins, namely their exploitation as sensitizers in optoelectronic nanodevices, such as excitonic solar cells,[9−11] due to their visible-light harvesting capabilities.

Anthocyanins occur in nature as glycosylated polyhydroxy and polymethoxy derivatives of 2-phenylbenzopyrylium cation or flavylium cation (Scheme 1) and differ in the number and position of hydroxyl and methoxyl groups along the structure, as well as in the identity, number, and position of the sugars attached to the carbon skeleton.[12] As observed in several experiments, both in vivo and in vitro,[13] anthocyanins undergo structural modifications and related color variations upon changing the environmental conditions, such as pH, concentration, temperature, presence of other flavonoids or metal cations. In aqueous solutions, anthocyanins may exist in several phases and charged states as shown in Scheme 1, the flavylium cation (AH^+), the quinonoidal base (A), the ionic quinonoidal anion (A^-), the carbinol pseudobase (B), and the chalcone (C). In very acidic media (pH < 3), the flavylium cation is the only stable species, characterized by a reddish color. The increase of pH up to neutral conditions (pH ∼ 6−8) induces a transition to the neutral quinonoidal form (A), associated with the loss of a proton, typically at the hydroxyl group positioned at C4′ (Scheme 1). At pH values higher than 8, a negative ionized base (A^-) is formed, through the removal of a second proton, typically at C7. This gives rise to bathochromic and hyperchromic shifts in the absorption spectra, which induce a color change toward bluish hues. In moderately acidic media (pH ∼ 3.5−6) another reaction may take place: the hydration of the flavylium cation to yield the colorless carbinol pseudobase (B). At a slower rate, this in turn can equilibrate to the open chalcone form (C). Notably, the reactions shown in Scheme 1 are reversible; therefore the changes of the pH present a tool to control the optical (color) properties of anthocyanins.

The possibility of tailoring their electronic and optical properties justifies the renewed interest in the anthocyanins due to their widespread applications. There is, however, a lack of adequate characterization of their intrinsic properties at a microscopic level. In fact, despite the plethora of experimental data, stemming from biological and agronomic fields, which gave a qualitative description of these molecules, a deep understanding of the intimate links between the anthocyanin structure and its properties is still missing. In particular, the diversity of the analyzed molecules of the experimental setups and environmental conditions produces a large variability in the results that prevents the comparison and the interpretation of the data. For instance, particularly important can be the choice of the buffer solution and of the counterions used to control pH and to neutralize the charged molecular ions. This lack of

* To whom correspondence should be addressed. Phone: +39-059-2055320. Fax: +39-059-2055627. E-mail: arrigo.calzolari@unimore.it.
† National Center on nanoStructures and bioSystems at Surfaces (S3) of CNR-INFM.
# Also at European Theoretical Spectroscopy Facility (ETSF).
‡ Università di Modena e Reggio Emilia.
§ CNR-IMEM, Parco Area delle Scienze.
|| The Hebrew University of Jerusalem.

10.1021/jp904966d CCC: $40.75
Published on Web 07/07/2009

SCHEME 1: Structural Transformations of Cyanidin-3-glucoside Molecule in Aqueous Solvent

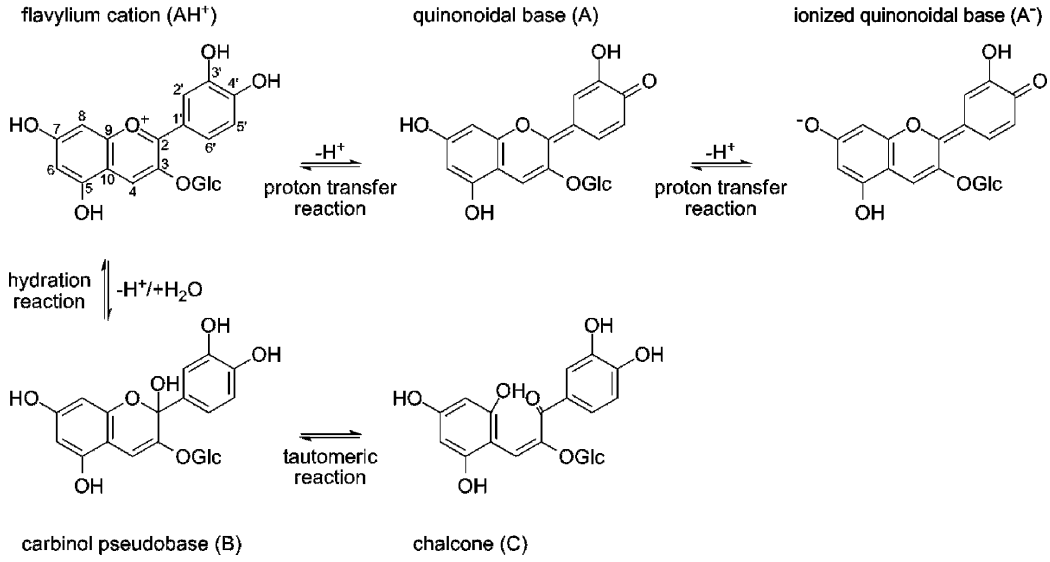

knowledge is also due to the unavailability of complete supporting theoretical studies. A proper description of the fundamental properties of the anthocyanins and the identification of the interaction mechanisms with the external world is crucial to exploit and control the properties of these molecules in nanotechnology and biomedical applications.

Here, we present a combined theoretical and experimental investigation of the optoelectronic properties of the natural cyanin dye (cyanidin-3-glucoside). Cyanin (Cya) is a red-colored anthocyanin widely present in nature, and it is considered one of the most promising targets for biomedical and energy applications.[9−11] In fact, despite its simple structure, cyanin possesses a catechol terminal group, proposed as the active chromophore in optoelectronic systems.[14] Furthermore, the −OHs linked to the chromophore provide useful anchoring sites on inorganic surfaces or larger biomolecules (e.g., nucleic acids and proteins).[8,15]

In the present study, we first supply a microscopic characterization of the structural and optoelectronic properties of cyanin molecules in different gas-phase configurations, that correspond to the structures occurring at the different pH values (Scheme 1). To this aim, we employ a fully ab initio approach in the framework of the static and the time-dependent density functional theory, and we validate our theoretical results by means of the direct comparison of the calculated results with the experimental data. Second, in view of the potential nanoscale applications we realize a prototypical optoelectronic device based on cyanin molecules, operating in electrochemical ambient conditions. We demonstrate the formation of controlled molecule/contact interfaces and we show, as a proof of concept, that the resulting photocurrent yield may be significantly enhanced by the addition of specific ligands to the electrolyte.

Our combined study allows us to unambiguously highlight the effects induced by the hydration and hydroxylation reactions on the intrinsic properties of cyanin, as well as the role of the attached sugar on the charge distribution, the optical gap, and the optical activity of lowest-energy excitations with its possible implications on luminescence quenching properties of the molecular dye arising from the presence of dark states. Our results demonstrate the persistence of the light-harvesting capability of cyanin, both in solution and in an electrochemical device configuration. This issue, along with the possibility of increasing the collected photocurrent, is particularly attractive for possible nanoscale applications, such as light sensors and photovoltaic solar cells.

2. Theoretical Results

Following the experimental observation that the glycosylated molecules are more stable than the corresponding aglycons,[9,13] we focus on the cyanidin-3-glucoside dyes in the five states reported in Scheme 1. The results for two key aglycon cyanidin phases (flavylium and carbinol), where the absence of the sugar affects the features of the molecule in very different ways, are reported in the Supporting Information.

In the analysis of the results we distinguish between the AH^+, A, A^- states, which are the results of subsequent proton transfer processes, and the B, C configurations that are associated to the hydration reaction.

2.1. Flavylium (AH^+) and Quinonoidal (A, A^-) Structures. After total-energy and atomic-force relaxation, the flavylium and quinonoidal A and A^- bases do not undergo remarkable structural distortions with respect to the starting planar geometry (see also Technical Details); the benzopyrylium unit maintains the initial planarity, while the catechol group only slightly rotates by $\theta_{321'2'} \leq 14°$, being that θ is the torsional angle between the benzopyrylium and the catechol ring. The sugar geometries remain instead mainly unchanged. Passing from cation to anion state, only the C−O distances relative to the oxidation sites reveal a partial contraction. Structural results for all configurations are summarized in Table 1.

Despite the different charge configurations, the AH^+, A, A^- configurations are isoelectronic with an even number of electrons, thus no structure has singly occupied molecular orbitals. The energy level distribution (Figure 1) shows that the three systems have very similar DFT HOMO−LUMO gaps ΔE_{HL} (the numerical values are reported in Table 1). From the comparison of the energy spectra (Figure 1), we note also a systematic downshift of the energy levels going from AH^+ to A^-, both for the occupied and empty states. This is consistent with the increase of the negative charge from flavylium to the anionic state.

The analysis of the single-particle molecular orbitals highlights interesting features. The frontier orbitals (a few selected ones are plotted in Figure 2) have a general π-character delocalized over the $C_6C_3C_6$ skeleton of the molecule, the

TABLE 1: Summary of Geometrical and Electronic Parameters of the Investigated Cyanidin-3-Glc (Atomic Subscript Labels as in Scheme 1)

		$d_{Cx\text{-}Ox}$ (Å)[b]								
	$\theta_{321'2'}$ (deg)[a]	d_{2-1}	d_{9-1}	d_{5-5}	d_{7-7}	$d_{3'-3'}$	$d_{4'-4'}$	$\langle d_{O-H}\rangle$ (Å)[c]	ΔE_{HL} (eV)[d]	μ (D)[e]
AH^+	14.2	1.37	1.37	1.36	1.36	1.36	1.35	0.98	1.51	
A	9.5	1.40	1.37	1.37	1.37	1.37	1.25	0.98	1.50	1.60
A^-	13.6	1.39	1.39	1.39	1.26	1.38	1.26	0.98	1.43	
B	98.2	1.46 (1.43)[f]	1.38	1.38	1.38	1.38	1.38	0.98	3.19	0.33
C	−19.4	−(1.28)[f]	1.33	1.38	1.37	1.37	1.37	0.98 (1.05)[g]	2.03	0.73

[a] $\theta_{321'2'}$ is the torsional angle between benzoperylium and catechol rings. [b] $d_{Cx\text{-}Ox}$ are the carbon−oxygen distances. [c] $\langle d_{O-H}\rangle$ is the average OH distance. [d] ΔE_{HL} is the HOMO−LUMO gap calculated at the DFT level. [e] μ is the modulus of the dipole moment vector of neutral structures. [f] The value between parentheses is the atomic distance between C_2 and the oxygen atom of adsorbed hydroxyl group O_h. [g] The value between parentheses is the atomic distance between O_1 and the hydrogen atom of adsorbed hydroxyl group H_h.

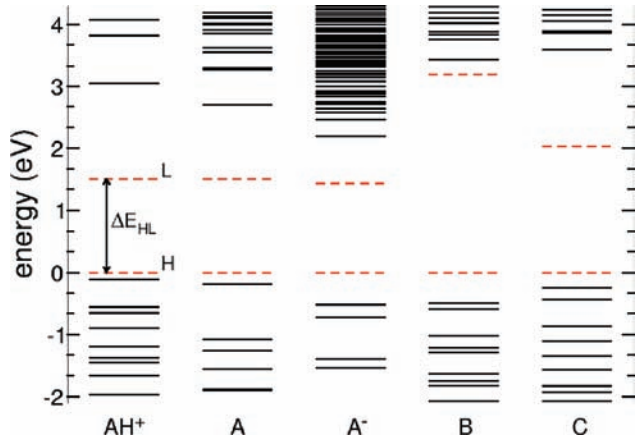

Figure 1. Schematic of DFT single-particle energy levels for Cya molecules. Red dashed lines marks the HOMO (H) and LUMO (L) states of molecules. Structural labels refer to Scheme 1. Zero energy reference is aligned to the HOMO state of each system.

LUMO state in particular has the same character in the flavylium and in both the quinonoidal bases. In contrast, the HOMO state of the flavylium cation has, surprisingly, a completely different symmetry, being strongly localized on the sugar moiety; the HOMO states for the quinonoidal bases A and A^- are fully delocalized on the aglycon part of the molecule. A rearrangement of the electronic states takes place. Sugar-localized orbitals, such as the AH^+ HOMO, are recognizable also among the quinonoidal orbitals, but at lower energies (namely HOMO−4 and HOMO−7 for neutral and anionic base respectively); conversely, the HOMO-1 state of AH^+ cation has the same character as the HOMO state of A and A^- structures.

In the case of flavylium, the electronic states stemming from the sugar group, which in similar biomolecular systems (e.g., nucleosides[16]) typically contribute to a lower part of the energy spectrum, are shifted high in energy for electrostatic reasons. The attractive interaction between the positively charged site (formally centered on the O_1 atom) and the dipole field induced by the lateral OH terminations gives rise to an electrostatic potential, anisotropically aligned from the hydroxyl group of the catechol ring to the opposite OH-group of the glucose sugar. This is responsible for the upward energy shift of the sugar-localized state of flavylium (see also Supporting Information).

It is also worth noticing the presence of σ-like states for the quinonoidal bases A (HOMO−1) and A^- (HOMO−1, HOMO−2), which are the result of proton transfer reactions, energetically separated by lower-energy π-states. In order to get more insight into the effects of the protonation and of the attached sugar, we investigated three further neutral quinonoidal systems, which differ by the position of the protonation and the glucose sites, and whose geometries are reported in Figure SI-2 (Supporting Information). The structural modifications do not yield remarkable modifications, and the resulting electronic properties are perfectly in agreement with those presented for the quinonoidal state (A) that we assume as the reference (for details see Supporting Information).

In Figure 3, we show the calculated absorption spectra (i.e., the dipolar strength functions) for the molecule in the three reference states: AH^+ (top), A (middle), and A^- (bottom). The spectra for the AH^+ and A are dominated by two major peaks in the low-energy region of the visible range; in the case of flavylium, the corresponding wavelengths are 579 and 452 nm, while for the quinonoidal base they are 532 and 416 nm. For the ionized base, only a single low-energy peak (564 nm) is preponderant in the visible region, although a much less intense structure is obtained near UV at 365 nm (marked with an arrow in Figure 3, see Discussion below). Higher energy absorption bands in the UV region do exist for the three configurations.

Besides the excitations corresponding to bright states (i.e., observable in the absorption spectra), the presence of dark states below the first bright ones (not observable) are particularly relevant in the identification of the possible mechanisms for the de-excitation process of these molecules. We analyze the energy and the character of the main excitations in terms of transitions between single-particle states, by means of the evaluation of the optical spectra in linear response and in the frequency domain,[17] (numerical values are reported in SI). The lowest-energy bright peaks originate from $\pi-\pi^*$ transitions, mainly associated with HOMO→LUMO transitions for A and A^- bases, and to (HOMO−1)→LUMO transition for AH^+, which have the same symmetry, in agreement with the single particle analysis presented above.

In the case of flavylium, the relevant sugar contributions to the electronic structure give rise to low energy charge transfer states (zero oscillator strength), as well as to an extra contribution at $\lambda = 512$ nm (vertical arrow in Figure 3), not observed in the other structures. This is confirmed also by the direct comparison with the absorption spectrum (dotted line, top panel) of the corresponding aglycon (see Supporting Information for further details). Notably, the presence of polar solvent and counterions may further shift the sugar-derived feature to a higher energy part of the spectrum. Thus, we can conclude that the sugar moiety, which is essential for energetic and electrostatic stabilization of the molecule, has only minor effects on the optical properties of the flavylium cation.

In the case of quinonoidal bases, a few dark states[18] are found to derive from $\sigma-\pi^*$ transitions, associated to the σ-like orbitals, localized around the protonated sites. Passing from the neutral to the ionized configuration, we observe depletion of optically active states below the HOMO (both HOMO−1 and HOMO−2

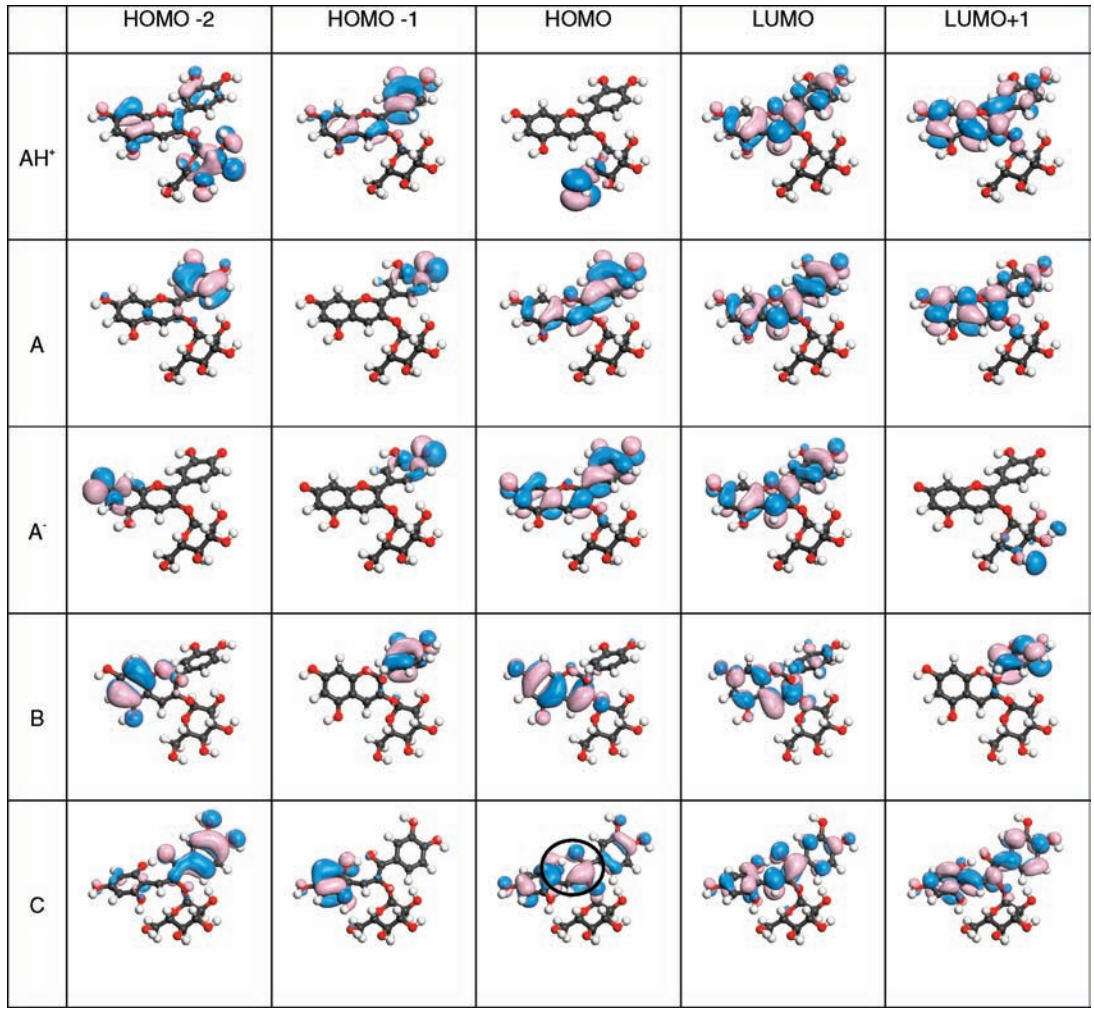

Figure 2. Charge density plots of selected frontier orbitals (HOMO−2, HOMO−1, HOMO, LUMO, LUMO+1) of cyanin molecules. Structural labels refer to Scheme 1.

have a σ-like character) and above the LUMO (LUMO+1 is localized on the sugar moiety), as shown in Figure 2. This results in a progressive reduction of the second visible peak of the spectra ($\lambda \sim 400$ nm), only partially compensated by the transition either from deeper valence or to higher conduction states (see Supporting Information Tables SI−III, SI−IV, and Figure 1).

Heuristically, these features may explain the color variation of Cya as a function of the external pH. In biological systems, we are not dealing with monochromatic (single frequency) spectra; on the contrary, the color of the dye is the result of the optical superposition of all the transmitted (i.e., not absorbed) light components in the visible range. The three Cya phases have two main absorption bands in the visible region, one at 530−580 nm and another at 410−440 nm, which correspond to blue-violet and yellow-orange transmitted light, respectively. While the contribution of the first edge is almost common to the three configurations, the second one progressively vanishes passing from flavylium AH^+ to ionized quinonoidal base A^- (i.e., increasing the pH). The massive superposition of the two contributions drives the color of flavylium toward reddish hues, while the predominance of a single peak for the ionized phase (A^-) is responsible for its blue-violet color. This is in qualitative agreement with the bathochromic shift, experimentally observed with the increase of the solution pH.[13]

We also note that the presence of dark states below the first bright excitation peak for all the three structures may favor

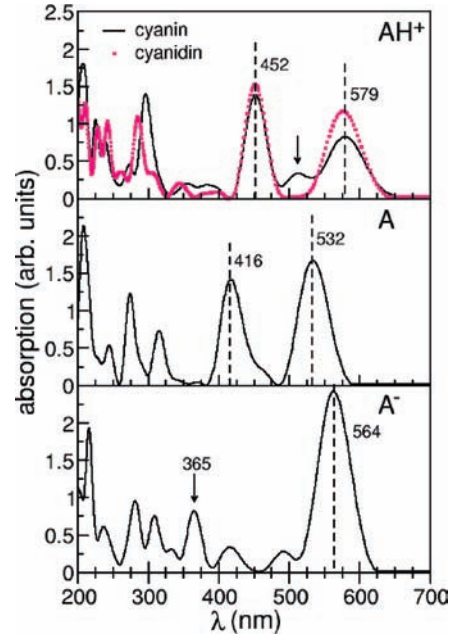

Figure 3. Calculated optical absorption spectra in the range 200−800 nm for (top) the glycosylated (black line) and aglycon (magenta dotted line) AH^+ flavylium; (middle) quinonoidal A; (bottom) anionic quinonoidal A^- structures. All the molecules are considered in the gas phase.

nonradiative mechanisms in de-excitation processes,[18] in agreement with the quenching of the photoluminescence signal, observed in the experiments.[1]

2.2. Carbinol (B) and Chalcone (C) Structures. The linkage of an extra hydroxyl group in the carbinol and chalcone states induces strong structural distortions. As reported in Table 1, we observe a severe lack of planarity due to the strong rotation of the catechol ring. Notably, the carbinol configuration B results to be energetically more stable than the chalcone C by only $\Delta E_{tot} = 37$ meV. Hereafter, we label O_h and H_h the oxygen and hydrogen atoms constituting the tethered hydroxyl group, respectively.

In the case of the carbinol pseudobase B, the formation of a covalent bond at site C_2 disrupts the conjugation of the pyrylium ring. In particular, the C_2 atom slightly displaces out of the benzopyrylium plane, rearranging in an almost tetrahedral configuration, associated with the elongation of the corresponding bond lengths. In the tautomeric chalcone geometry, the hydrogen H_h migrates from the OH-group to the O_1 site, opening the pyrylium ring and forming a $C_2{=}O_h$ termination. Breaking the ring further modifies the structure that increases its out-of-plane distortion. The H_h hydrogen forms a covalent bond with O_1 and a hydrogen bond with O_h. In order to optimize the $O_1{-}H_h{\cdots}O_h$ hydrogen bond, the rotation of the $C_2{-}O_h$ and $C_2{-}C_3$ bonds is mainly responsible for the large torsion of the attached catechol ring.

The absence of planarity is also reflected in the single particle orbitals of the B and C molecules (see Figure 2). The frontier states maintain a π-like character but are more localized on specific subregions of the molecule. Indeed, while the HOMO (HOMO$-$1) states of the quinonoidal (flavylium) bases are fully delocalized over the entire $C_6C_3C_6$ structure, in the case of carbinol the HOMO and HOMO$-$2 states are centered on the benzopyrylium and the HOMO$-$1 over the catechol ring. LUMO and LUMO+1 have also different symmetries and sugar-derived states are present only at lower energies. Notably, the covalent nature of the $C_2{-}$OH bond is confirmed by the formation of a bonding state below 2.5 eV under the HOMO level in the energy spectrum (not shown). The localization process is further evident in the C structure especially in the HOMO$-$1 and HOMO$-$2 states, where the effect of the ring-opening is evident. The HOMO shows a small but not negligible charge density component surrounding the $O_1{-}H_h{-}O_h$ atoms (see circle in Figure 2), in agreement with the formation of a H-bond.

The calculated absorption spectra, shown in Figure 4, are very different for carbinol (top panel) and chalcone (bottom panel) respectively. Carbinol does not present bright absorption contributions in the visible range, having the lowest-energy peak at $\lambda = 337$ nm in the UV region. This excitation derives from a $\pi{-}\pi^*$ transitions from HOMO to LUMO and LUMO+2 states, broadly delocalized over the benzopyrylium ring. The strong localization of LUMO+1 state over the catechol group generates dark charge transfer states in the near-UV region.[18]

More subtle is the effect of the attached glucose fragment: Despite the similar symmetries of the ground state molecular orbitals (compare Figure 2 and Supporting Information SI-5), the dipole field induced by sugar provides a different energy level distribution (i.e., reduces the gap) that remarkably modifies the threshold of the adsorption spectra. This is evident in Figure 4, where the calculated spectrum for the aglycon structure (dotted line) is very similar to the corresponding glycosylated one, except for the position ($\lambda = 396$ nm) and the intensity of the first bright excitation, which causes a remarkable blue shift of the first peak.

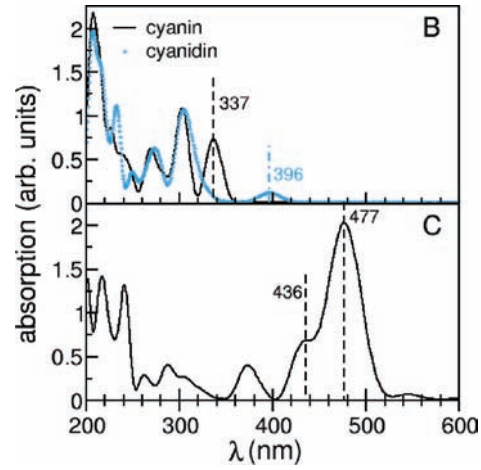

Figure 4. Calculated optical absorption spectra in the range 200−600 nm for (top) carbinol B phase with (black line) and without (dotted blue line) attached sugar. (bottom) Glycosylated chalcone C structures. All the molecules are considered in the gas phase.

TABLE 2: Summary of Lowest-Energy Absorption Peaks as a Function of pH, for Cya Molecules in Solution (No Substrate) with and without the Addition of Mercaptophenyl Boronic Acid

	pure cyanin[a] λ (nm)				Cya + boronic acid[b] λ (nm)	
pH	I (exp)	I (theo)	II (exp)	II (theo)	I (exp)	II (exp)
4	512	579	429	452	523	
6	539		430		550	
7.4	578	532	435	416	554	469
9	570	564	380	365[c]	552	474

[a] Cyanidin-3-glucoside concentration = 50 μM. [b] Mercaptophenyl boronic acid concentration = 500 μM. [c] Peak marked with vertical arrow in Figure 3.

The chalcone spectrum is characterized by a strong peak at $\lambda = 477$ nm with a marked shoulder at 436 nm that is in the visible region and corresponds to a yellowish color, which is in agreement with the experimental results.[13] The higher energy contributions are in the UV region. The bright excitations have a $\pi{-}\pi^*$ character, stemming from transitions from occupied frontier orbitals to LUMO state. The other virtual states (LUMO+1, LUMO+2, etc.) lie in a higher energy range (see also Figure 1) and do not contribute to the absorption spectrum in the range considered here. No dark or charge transfer states are detected for this system, favoring radiative de-excitation processes and a more intense photoluminescence activity.

3. Experimental Results

We first characterize the optical spectra of the cyanin molecules, freely diluted (50 μM) in different buffer solution pHs (4, 6, 7.4, and 9), at room temperature. In Table 2 we report the main optical features of Cya as obtained experimentally for the free molecule in different buffer solutions to control pH; the corresponding theoretical values are also indicated for comparison. To our knowledge, this thorough analysis is proposed for the first time. As one can see there is a nice agreement between the theoretical and the experimental data, in the different conditions. In particular, the main peaks in the visible range are closely reproduced for all moieties. The minor differences between the calculated and experimental peak

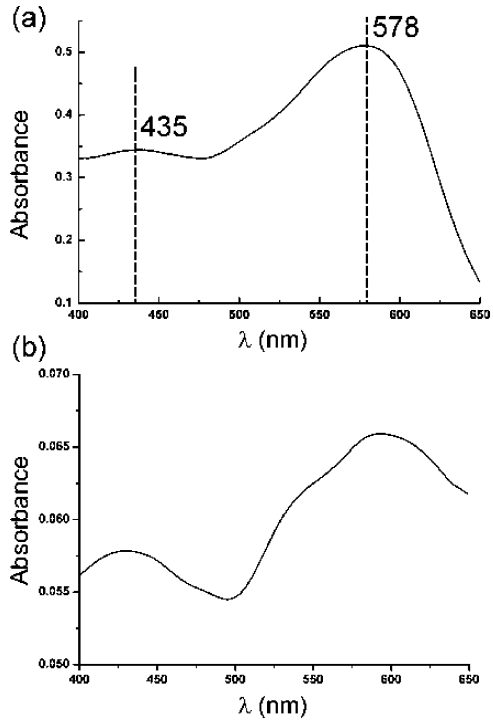

Figure 5. Experimental absorption spectra for (a) cyanin, 1×10^{-4} M, in a 0.1 M phosphate buffer solution, pH = 7.4; (b) cyanin linked through the boronic acid ligand to a semitransparent Au electrode, Scheme 2a. The spectrum was obtained by subtracting the spectrum of the bare Au slide prior to the modification from the spectrum of the surface after modification with cyanin.

positions may be ascribed to the presence of the aqueous solvent in the experimental system. This is a remarkable result, since it allows us to directly compare the intrinsic absorption properties of Cya (gas phase) with those of the molecule in solution, even though we cannot exclude that the explicit presence of a polar solvent and of the counterions in the buffer solution might have stronger effects in the case of the charged configurations (e.g., flavylium cation, see Discussion below).

The specific case of measured optical spectrum at pH = 7.4 is depicted in Figure 5a. It consists of two bands in the visible region, one high intensity absorbance band at $\lambda = 578$ nm and a low intensity absorbance band at $\lambda = 435$ nm. The presence of the two peaks, along with their energy position and relative intensity compare very well with the calculated spectrum for the quinonoidal phase A (Figure 4), in agreement also with the neutral pH. However, since the high intensity peak (578 nm) is quite spread in energy, we cannot exclude that the measured spectrum contains also a partial contribution from the flavylium ions that may coexist in solution, as minority component at the neutral pH. This would not be in contrast with the theoretical findings due to the similarity of the calculated spectra for AH^+ and A configurations (Figure 4).

In view of possible nanoscale applications, we analyze the light harvesting capabilities and the photocurrent-generation properties of Cya when it is connected to a conductive substrate (gold) to form an operating electrochemical device. In such systems, the generation of photocurrent is strongly dependent on the destructive charge recombination. Thus, in order to reduce the electron−hole recombination due to the fast electron transfer from the metal to the molecule we build up the Cya/gold contact through an intermediate donor−acceptor boronic acid spacer, which ensures a stable anchorage to the surface and avoids the charge back-donation from the Au contact. Furthermore, we

SCHEME 2: Different Cyanin Configurations Associated with Electrodes for Photocurrent Generation[a]

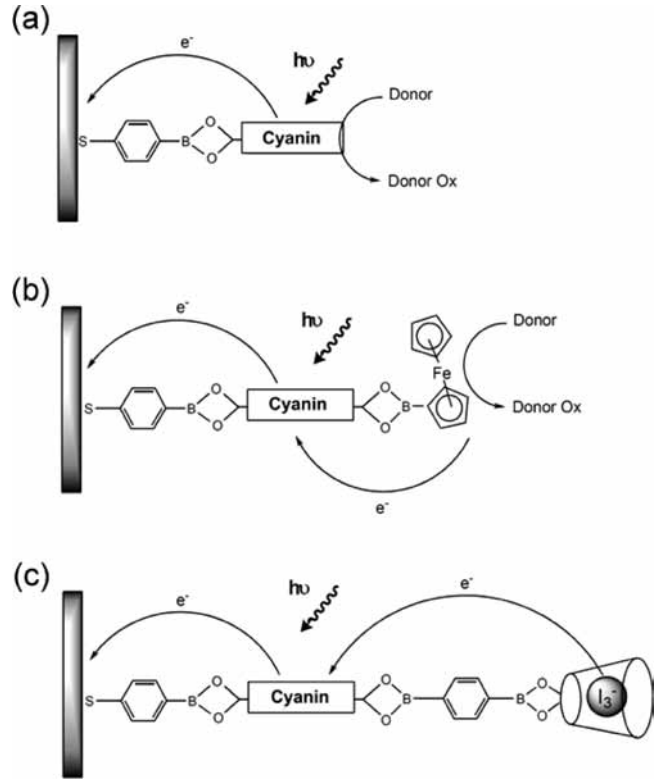

[a] (a) Cyanin linked to a Au electrode through a boronic acid ligand; (b) a cyanin-modified electrode in which the chromophore is further linked to a ferrocene unit through a boronic acid ligand. The ferrocene units act as electron donors for the valence band holes and they mediate the oxidation of the solution-solubilized electron donor. (c) A cyanin-modified Au electrode in which the chromophore is linked to a β-CD through a di-boronic acid unit. The β-CD provides a receptor unit for I_3^-, which serves as an electron donor for the valence band holes.

show how it is possible to enhance the reducing effect of the electrolyte (i.e., enhance the photocurrent) protecting the other terminations of the dye with proper functional groups.

We consider three representative configurations (illustrated in Scheme 2). As a preliminary step, we analyze the optical properties of Cya upon the exposure to mercaptophenyl boronic acid, 500 μM, in water solutions at different pHs. These results are reported in Table 2; the peak position is hardly affected by the inclusion of boronic acid in solution, indicating a weak Cya-ligand coupling. The only remarkable modification occurs at basic pH, where the highest energy peak of A^- is red shifted to visible; this may be assigned to boronic-acid instabilities in this condition. Hereafter, experimental measurements are taken at neutral conditions (pH = 7.4).

Once achieved that the boronic acid hardly affects the Cya properties, we make use of the spontaneous ligation of the boronic acid ligand to geminal diol functionalities to integrate Cya with metallic electrodes. Cyanin includes two such functions, the catechol ring, directly linked to the chromophore moiety, and the monosaccharide unit. In the first configuration (Scheme 2a), mercaptophenyl boronic acid is assembled on a gold electrode and the dye is subsequently linked to the boronic acid ligand. As the redox features of the surface linked Cya are similar to those of the aglycon cyanidin chromophore (see Supporting Information, Figure SI-6), which lacks the monosaccharide moiety, we assume that the catechol ring acts as the active group in coordinating to the boronic acid monolayer.

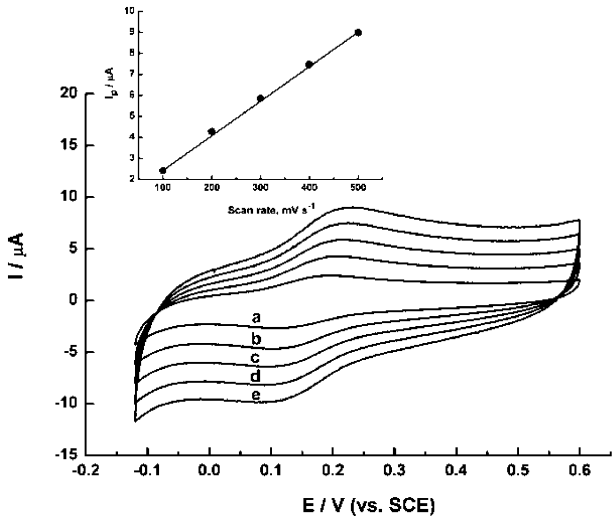

Figure 6. Cyclic voltammograms corresponding to a Au electrode modified with cyanin. Scan rates are (a) 100; (b) 200; (c) 300; (d) 400; and (e) 500 mV s^{-1}. Inset: The plot of the anodic peak current as a function of the scan rate. All measurements were performed in a phosphate buffer, 0.1 M, at pH = 7.4.

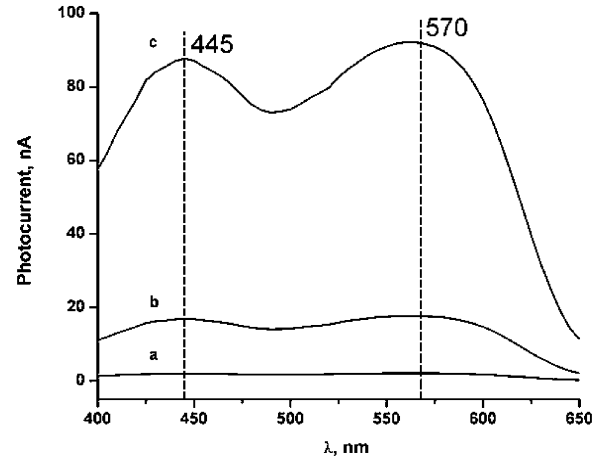

Figure 7. Photocurrent action spectra generated by the different cyanin configurations. (a) Cyanin linked to a Au electrode through a boronic acid ligand, Scheme 2a; (b) a cyanin-modified electrode in which the chromophore is further linked to a ferrocene unit trough a boronic acid ligand, Scheme 2b; (c) a cyanin-modified Au electrode in which the chromophore is linked to a β-CD through a diboronic acid unit, Scheme 2c. All measurements were performed under Ar in a phosphate buffer solution, pH = 7.4, that included 5 mM I_3^- as an electron donor.

The formation of the metal/dye interface is characterized by means of cyclic voltammetry measurements. The cyclic voltammograms of the Cya monolayer, as a function of scan rate, are depicted in Figure 6. A quasi-reversible redox wave is observed at $E^\circ = 0.15$ V versus SCE, pH = 7.4. The anodic (or cathodic) peak currents reveal a linear dependence on the scan rate, consistent with a surface-confined redox-species (inset of Figure 6). The coulometric analysis of the redox wave indicates a surface coverage of Cya on the electrode that corresponds to ca. 1.1×10^{-11} mole·cm^{-2}.

The spectrum of cyanin bound to the Au surface (Figure 5b) was characterized by the immobilization of the molecule on a semitransparent Au surface and by the subtraction of the spectrum of the clean surface. The resulting spectrum almost coincides with that observed in solution (Figure 5a, and Table 2), showing that the binding to the electrode does not perturb the intrinsic absorption properties of the molecule that consequently may be assumed as simple reference in the following applications.

In the second configuration, Scheme 2b, ferrocene boronic acid is ligated to the glucose moiety of cyanin. A quasi-reversible single-electron peak, associated with the ferrocene units is observed in the cyclic voltammograms (Supporting Information, Figure SI-7). The coulometric analysis of the redox wave indicates a surface coverage of ferrocene units that corresponds to 8.6×10^{-12} mole·cm^{-2}.

The photocurrents generated by the different electrode modifications are measured in the presence of I_3^- as a reversible, nonsacrificial, electron donor. While the configuration in Scheme 2a (i.e., Cya monolayer only) does not provide any measurable photocurrent (Figure 7, curve a), the covalent tethering of the ferrocene units to the Cya chromophore results in a measurable photocurrent, ca. 17 nA (Figure 7, curve b). The formation of the photocurrent by the cyanin-ferrocene monolayer system is attributed to charge separation that occurs in the dyad structure of the monolayer. The photoexcitation of the Cya monolayer in configuration (a) results in a charge injection into the Au electrode and the intermediary formation of the oxidized cyanin$^{\cdot+}$. The diffusional oxidation of I_3^- is inefficient and cannot compete with the back electron transfer from the electrode to cyanin$^{\cdot+}$. As a result, no measurable photocurrent is observed. The covalent attachment of the ferrocene unit, which acts as electron donor, results in the oxidation of the ferrocene by the photogenerated cyanin$^{\cdot+}$. This leads to the spatial charge separation of the electron (injected into the electrode) and the "hole" preserved in the ferrocene units. The stabilization of the redox products against recombination allows the subsequent oxidation of I_3^- by the ferrocenyl cation units, and the formation of the steady state photocurrent.

The third configuration, Scheme 2c, includes the primary tethering of the dye to the boronic acid monolayer followed by the covalent attachment of β-cyclodextrin (CD) to the chromophore, using 1,4-phenyl diboronic acid as bridging units. β-cyclodextrin is a cyclic oligosaccharide consisting of seven glucose units linked by 1−4 glycoside bonds. It includes a cavity that associates organic or inorganic substrates. Furthermore, it binds effectively I_3^-, $K_a = 6.5 \times 10^2$ M^{-1}, and thus concentrates I_3^- at the vicinity of the Cya chromophore; Figure 7, curve c shows the photocurrent action spectrum generated by the system. Intensified photocurrents, $I = 88$ nA (at $\lambda = 445$ nm) and $I = 92$ nA (at $\lambda = 570$ nm), are observed. The high photocurrents are attributed to the effective scavenging of the oxidized chromophore, cyanin$^{\cdot+}$, by the I_3^- concentrated at the electrode surface. The high local concentration of I_3^- effectively reduces the photogenerated oxidized cyanin$^{\cdot+}$ in a process that competes with the degrading recombination. Further support that the concentration of I_3^- at the electrode surface leads to the high photocurrent value is obtained by following the photocurrents upon the inhibition of I_3^- binding to the β-cyclodextrin units by adding adamantane carboxylic acid, to the system. Adamantane carboxylic acid, competitively binds to β-cyclodextrin, $K_a = 4.3 \times 10^4$ M^{-1}, reducing the concentration of I_3^- at the electrode surface, which results in a reduction of the generated photocurrent (see Supporting Information).

Interestingly, the photocurrent action spectra reveal two photocurrent peaks at 445 and 570 nm, consistent with the absorbance features of cyanin (Figure 5). Knowing the light intensity adsorbed by the Cya monolayer, we estimate the quantum yield for generation of the photocurrent to be $\phi = 1.7\%$ for both the $\lambda = 445$ nm and $\lambda = 570$ nm wavelengths for the system consisting of the cyanin-β-cyclodextrin-I_3^-

system, Scheme 2c, and $\phi = 0.35\%$ for the cyanin-ferrocene-I_3^- system (Scheme 2b). The quantum yields at the two wavelengths 445 and 570 nm show similarities, while lower absorption intensity is observed for the molecular monolayer at 445 nm, Figure 5b. This is explained by the different lifetimes of the photoexcited states. The electronic state corresponding to the excitation of Cya at $\lambda = 445$ nm has a lifetime of $\tau = 0.85$ ns, while the excitation of the band at $\lambda = 570$ nm exhibits a lifetime of $\tau = 0.60$ ns. The longer lifetime of the state absorbing at $\lambda = 445$ nm results in enhanced charge injection which compensates for the lower absorption intensity. We remark that, even though the measured quantum yield is still low in its absolute value, especially in comparison with other long studied systems (e.g., fully inorganic[19] and hybrid-junctions[20] materials), our results demonstrate the capability of increasing the current generation controlling, at the microscopic level, the mechanisms of charge separation at the different interfaces that compose the electrochemical device.

In the different systems, we assumed that the catechol moiety of Cya binds to boronic acid monolayer, and that the saccharide units participate in the linkage to boronic acid bridge in the second step. This assumption is supported by the observation that the cyanidin chromophore that lacks the saccharide moiety, binds to the base boronic acid monolayer, similarly to Cya. In fact, the cyclic voltammogram and surface coverage of the cyanidin are similar to those of the glycosylated Cya and demonstrate a linear dependence between the anodic or cathodic peak currents and the scan rate, indicating that the aglycon is connected to the surface (Supporting Information, Figure SI-6).

4. Discussion

In the previous analysis, we mentioned how differently the sugar fragment may affect the properties of cyanins; the effect of glucose is not ubiquitous and varies on the base of the configuration and of the environment. On the structural side, the high density of hydroxyl groups and the steric hindrance of glucose markedly influence the stability and the final geometry of the single molecules. This effect is more pronounced for configurations such as flavylium or chalcone, which exhibit very high inhomogeneous charge distribution. The nonplanarity of cyanin also constrains the stacking and the molecule−molecule interactions that are expected to be important in the realization of self-assembled monolayers. In principle, the presence of −OH harpoons, including the sugar ones, may furnish anchoring sites for the direct adsorption to inorganic substrates, alternative to the catechol.

On the optical side, the presence of the sugar unit, excluded in previous calculations,[11,16] introduces dark states and impacts the shape of the absorption spectrum; in the AH^+ state of cyanin, it induces the appearance of an extra-peak between the two lowest-energy ones of the corresponding aglycon, while for the B state it causes a blue shift of the first peak. Incidentally, we also note that in experimental findings the best photocurrent response is obtained in the presence (in solution) of β-cyclodextrin that is itself a glucose chain aggregate. The microscopic mechanisms that rule the interaction and the charge injection in CD fragment are not completely understood and require further investigations.

Another debated question deals with the shape and the number of absorption bands in the visible ranges for the single molecule in solution. Although earlier experimental results[9,13,21] reported a single peak, more recent data[10a] identified two major absorption bands. Our results support the latter characteristic. On the theoretical side, recent TDDFT simulations also show two absorption components at 410 and 532 nm for the aglycon quinonoidal base,[11] very similar to our results. In contrast, previous theoretical results,[22] based on semiempirical ZINDO approach, were not able to reproduce the complexity of the Cya molecule, reporting a single absorption peak at $\lambda = 474$ nm.

The experimental data reported so far and obtained in acidic solution (pH < 4) for flavylium cation show a first absorption peak at $\lambda = 510-520$ nm,[9,10] that is, in agreement with our experimental findings (Table 2) but at higher energy with respect to our theoretical results (Figure 4, top panel). However, this blue shift is not dramatic since it is well inside the range of TDDFT accuracy (see technical details) and may be also driven by the presence of the surrounding polar solvent. The effect of the solution is reasonably different in acidic or basic conditions, because of the different neutralization of the counterions from the buffer solution. The thorough comparison presented in this work, along with the good experimental-theoretical agreement for the different molecular charge states, reasonably validates a posteriori also the theoretical results related to the other cyanin configurations.

In the case of cyanin adsorption on semiconducting TiO_2 nanoparticles,[9,10] some modifications of the absorption spectra further demand for a deeper understanding. Despite the specific details, such experiments first characterize the absorption of single molecules in acidic conditions (pH < 4), which correspond to the flavylium cation phase ($\lambda = 510-520$ nm). Then, after the molecular binding on metal-oxide nanoparticles, a strong red shift to $\lambda = 550-570$ nm is reported and associated to a molecular transition to the protonated quinonoidal configuration. From one hand, these absorption values well compare with what obtained in our work; on the other hand, the underlying physical processes are not completely understood. At variance with our experimental results, where the experimental conditions (pH, solvent, counterions) and the use of boronic-acid tinkers ensure a weak molecule/surface coupling (Figure 5), in the previous experiments the direct role of the metal-oxide surface is not completely controlled. It is very possible that Cya underwent a phase transition caused by the strong coupling with the metal-oxide. However, since in the case of TiO_2 there were not specific characterizations of the interface, it is not evident how the changes in the spectral features have to be ascribed only to the molecular modifications instead of a molecule/surface mixed contribution.

5. Conclusions

In this study we present a combined theoretical and experimental study of the optoelectronic properties of the cyanidin-3-glucoside molecule in both the separated states and surface-confined configurations.

The theoretical analysis is focused on the microscopic characterization of the intrinsic properties of the dye, which is the necessary step also for the interpretation of the subsequent optoelectronic applications. We analyze Cya in the gas phase at different configurations associated to the experimental pH modifications, and we show the effects of the hydration and hydroxylation reactions as well as of the attached sugar on the ground and excited states. In particular, the visible-light harvesting capability of the dye is demonstrated. The reported results are then validated by the experimental data at controlled pH.

We exploit the optical properties of the dye to assemble a photoelectrochemical cell, where Cya is the optical-active element for the photocurrent generation. Our results demonstrate

a control over the generation of photocurrents through the photoexcitation of Cya, and the assembly of organized photosensitizer-electron donor assemblies, while implementing the nonsacrificial I_3^- electron donor. In our configuration, we tailor a photosensitizer-ferrocene dyad monolayer on the electrode surface. The electron transfer cascade in the system led to charge separation and the ferrocenyl cation-mediated oxidation of I_3^-. In the second configuration, a photosensitizer-β-cyclodextrin receptor monolayer is assembled on the electrode. The supramolecular concentration of I_3^- in the cavities of the receptor concentrates the donor at the photosensitizer. This enabled the effective scavenging of the oxidized photosensitizer product, thus competing with the back electron transfer of the photoproduct and allowing an effective photocurrent generation in the system.

The results of this joint theoretical and experimental investigation point out the different contributions and the microscopic mechanisms that regulate both the light adsorption and charge separation in such complex hybrid device, based on the natural Cya dye.

6. Technical Details

Theory. We carry out first principles quantum mechanical calculations on the electronic and optical properties of the cyanidin-3-glucoside molecule in different gas phase structural configurations. The direct atomistic description of the electronics of the overall system constituted by molecules and solvent, as found in nature, as well as the kinetics of the hydration processes is a terrific theoretical challenge, since one should take explicitly into account the molecule and the water solution as a function of the H^+ concentration. This problem would require an effort that goes beyond state-of-the-art ab initio calculations; thus we opt for the alternative approach where the environment is taken into account for what concerns its effect on the molecular structure. We describe from first-principles the optoelectronic properties of the Cya in all the different gas phase configurations that correspond to the structures occurring at the different pH values of the solvent (Scheme 1).

The ground-state electronic structure of the systems is obtained by means of total-energy and forces simulations, based on density functional theory (DFT) calculations, as implemented in the PWscf code.[23] Computational details are reported in ref 24. For neutral configurations, the total dipole moment is calculated in terms of maximally localized Wannier functions, using the WanT code.[25] As the experimental X-ray characterization of the pure Cya crystal is not available, we prepare the starting configurations using a standard chemical builder. The resulting molecules are characterized by a planar $C_6C_3C_6$ skeleton, in agreement with experimental configuration adopted by cyanin in more complex enzymatic compounds.[26] Each configuration is optimized, then the corresponding ground state properties are collected.[27]

The optical absorption spectra of configurations, optimized at the DFT level, are computed within time-dependent density functional theory (TDDFT)[28] by using a real-space, real-time approach to solve the time dependent Kohn−Sham equations as implemented in the computer code octopus;[29] computational details are reported in ref 30. The difference between single-particle DFT energy levels is renormalized within TDDFT through the Coulomb exchange-correlation terms that properly include contributions from virtual particle-hole excitations. The reported dipolar strength functions are calculated by averaging the dynamical polarizabilities along the three spatial directions. By plotting separately the curves for the different light polarizations, the absorption spectrum is highly anisotropic, since the dipolar strength function for perpendicular polarization is one order of magnitude smaller than the one calculated for in-plane polarizations.

The real-time approach has numerical advantages since it does not require the calculation of the unoccupied states and it has been successfully applied to clusters and biomolecules (e.g., DNA bases and protein chromophores) with a typical accuracy of 0.2−0.3 eV ($\Delta\lambda \sim 60$ nm).[31]

In addition, we calculate also the absorption spectra in the energy domain by identification of the pole structure of the linear response function, solving the Casida's eigenvalue equations.[17] This latter approach is equivalent to the former one when solving the time-dependent Kohn−Sham equations in the linear response regime. Within this formalism, it is possible to qualitatively assign the character of each (bright and dark) excitations, in terms of Kohn−Sham single-particle single-hole excitations (Casida's ansatz).[17]

Experiments. We measure the optical absorption and photocurrent spectra of cyanin molecules freely diluted in aqueous buffer solutions as well as attached to gold electrodes in different electrochemical configurations, as reported in Scheme 2. The clean Au slides are reacted with mercaptophenyl boronic acid, 50 mM, in ethanol solution for a time interval of 12 h and then with a 0.1 M phosphate buffer solution at pH = 7.4 that includes 0.1 mM cyanin chloride for 2 h. For the preparation of the cyanin/ferrocene electrode assembly, the cyanin-modified Au electrode is further reacted for 2 h with a phosphate buffer solution that includes 10 mM ferrocene boronic acid. Cyanin/β-cyclodextrin (β-CD) electrodes are prepared by reacting the cyanin-modified Au electrode for 1 h with a phosphate buffer solution that included 10 mM benzene-1,4-diboronic acid, and subsequently linking the β-CD receptor unit by reacting the resulting electrode with a phosphate buffer solution that included 10 mM β-CD for 1 h. Following the modifications, the electrodes were rinsed with a phosphate buffer solution to remove any nonspecifically bound reagents.

Instrumentation: Photoelectrochemical experiments were performed using a photoelectrochemical system that included a 300 W Xe lamp (Oriel, model 6258), a monochromator (Oriel, model 74000, 2 nm resolution), and a chopper (Oriel, model 76994). The electrical output from the cell was sampled by a lock-in amplifier (Stanford Research model SR 830 DSP). The shutter chopping frequency was controlled by a Stanford Research pulse/delay generator model DE535. The currents were measured between the modified Au working electrode and a Pt wire ($d = 1$ mm) counter electrode. Cyclic voltammetry experiments were performed using a PC-controlled (Autolab GPES software) potentiostat (μAutolab, type III). A graphite rod ($d = 5$ mm) was used as the counter electrode, and a saturated calomel electrode (SCE) was taken as the reference. Absorption spectra were recorded using a UV/vis spectrophotometer (Shimadzu UV2401PC).

Acknowledgment. We thank Giancarlo Cicero, Stefano Corni, and Elisa Molinari for fruitful discussions. This work was funded in part by EU (sixth Framework Program) through the projects PROSURF, FP6-NEST-028331, and the NanoSci-ERA (NanoLICHT project). Access to the CINECA supercomputing facilities was granted by CNR-INFM.

Supporting Information Available: This material is available free of charge via the Internet at http://pubs.acs.org.

References and Notes

(1) Brouillard, R. Flavonoids and flower color. In *The Flavonoids*; Harborne, J. B., Ed.; Chapman and Hall Ltd: London, 1988; pp 525−538.

(2) (a) Gonnet, J.-F. *Food Chem.* **1998**, *63*, 409. (b) Gonnet, J.-F. *Food Chem.* **1999**, *66*, 387. (c) Gonnet, J.-F. *Food Chem.* **2001**, *75*, 473.

(3) McGhie, T. K.; Rowan, D. R.; Edwards, P. J. *J. Agric. Food Chem.* **2006**, *54*, 8756.

(4) Parry, J.; Su, L.; Moore, J.; Cheng, Z.; Luther, M.; Rao, J. N.; Wang, J.-Y.; Yu, L. L. *J. Agric. Food Chem.* **2006**, *54*, 3773.

(5) He, J.; Rodriguez-Saona, E.; Giusti, M. M. *J. Agric. Food Chem.* **2007**, *55*, 4443.

(6) Zheng, W.; Wang, Y. *J. Agric. Food Chem.* **2003**, *51*, 502.

(7) Stintzing, F. C.; Stintzing, A. S.; Carle, R.; Frei, B.; Wrolstad, R. E. *J. Agric. Food Chem.* **2002**, *50*, 6172.

(8) (a) Kong, J.-M.; Chia, L.-S.; Goh, N.-K.; Chia, T.-F.; Brouillard, R. *Phytochem.* **2003**, *64*, 923. (b) Galvano, F.; La Fauci, L.; Lazzarino, G.; Fogliano, V.; Ritieni, A.; Ciappellano, S.; Battistini, N. C.; Tavazzi, B.; Galvano, G. *J. Nutr. Biochem.* **2004**, *15*, 2.

(9) Cherepy, N. J.; Smestad, G. P.; Grätzel, M.; Zhang, J. Z. *J. Phys. Chem. B* **1997**, *101*, 9342.

(10) (a) Hao, S.; Wu, J.; Huang, Y.; Lin, J. *Sol. Energy* **2006**, *80*, 209. (b) Sirimanne, P. M.; Senevirathna, M. K. I.; Premalal, E. V. A.; Pitigala, P. K. D. D. P.; Sivakumar, V.; Tennakone, K. *J. Photochem. Photobiol., A* **2006**, *177*, 324. (c) Wongcharee, K.; Meeyoo, V.; Chavadej, S. *Sol. Energy Sol. Cells* **2007**, *91*, 566. (d) Tennakone, K.; Kumara, G. R. R. A.; Kumarasinghe, A. R.; Wijayantha, K. G. U.; Sirimane, P. M. *Semicond. Sci. Technol.* **1995**, *10*, 1698.

(11) Meng, S.; Ren, J.; Kaxiras, E. *Nano Lett.* **2008**, *8*, 3266.

(12) Gao, L.; Mazza, G. *J. Food Sci.* **1994**, *59*, 1057.

(13) (a) Brouillard, R.; Dubois, J. E. *J. Am. Chem. Soc.* **1977**, *99*, 1359. (b) Brouillard, R.; Delaporte, B. *J. Am. Chem. Soc.* **1977**, *99*, 8461. (c) Brouillard, R.; Delaporte, B.; Dubois, J. E. *J. Am. Chem. Soc.* **1978**, *100*, 6202. (d) Brouillard, R. *Phytochem.* **1983**, *22*, 1311.

(14) Duncan, W. R.; Prezhdo, O. V. *Annu. Rev. Phys. Chem.* **2007**, *58*, 143.

(15) Sarma, A. D.; Sharma, R. *Phytochemistry* **1999**, *52*, 1313.

(16) Barnett, R. N.; Cleveland, C. L.; Joy, A.; Landman, U.; Schuster, G. B. *Science* **2001**, *294*, 567.

(17) Casida, M. E. In *Recent Developments and Applications of Modern Density Functional Theory*; Seminario, J. M., Ed.; Elsevier Science: Amsterdam, 1996; pp 391−439.

(18) At the current TDDFT level, the identification of charge transfer transitions suffers from a lower accuracy since a local or gradient-corrected exchange-correlation functional is used. See also (a) Dreuw, A.; Weisman, J. L.; Head-Gordon, M. *J. Chem. Phys.* **2003**, *119*, 2943. (b) Gritsenko, O.; Baerends, E. J. *J. Chem. Phys.* **2004**, *121*, 655.

(19) Slaoui, A.; Collins, R. T. Advanced Inorganic Materials for Photovoltaics. *MRS Bull.* **2007**, *32*, 211–255.

(20) (a) Crabtree, G. W.; Lewis, N. S. *Phys. Today* **2007**, *60*, 37−42. (b) Kamat, P. V. *J. Phys. Chem. C* **2007**, *111*, 2834. (c) Snaith, H. J.; Schmidt-Mende, L. *Adv. Mater.* **2007**, *19*, 3187.

(21) Harbore, J. B. *Biochem. J.* **1958**, *70*, 22.

(22) Pereira, K. G.; Galembeck, S. E. *Spectrochim. Acta, Part A* **1998**, *54*, 339.

(23) Quantum-ESPRESSO is a community project for high-quality quantum-simulation software, based on density-functional theory, and coordinated by Paolo Giannozzi. See www.quantum-espresso.org and www.pwscf.org.

(24) We adopt gradient-corrected PBE (Perdew, J. P.; Burke, K.; Ernzerhof, M. *Phys. Rev. Lett.* **1996**, *77*, 3865) exchange-correlation functional and ab initio pseudopotentials (Vanderbilt, D. *Phys. Rev. B* **1990**, *41*, 7892). The single-particle electronic wavefunctions (charge densities) are expanded in a planewave basis set up to an energy cutoff of 25 Ry (200 Ry). The flavylium cation AH^+ (anionic base A^-) is calculated in a positively (negatively) charged cell, dropping (adding) one electron from (to) the total amount; instead, all the other systems are neutral. We simulate isolated systems using large periodically repeated supercells where molecules are separated from adjacent replica by a vacuum layer of ∼10 Å in each direction. For each structure, the metastable configuration is obtained optimization procedure until the forces on all atoms are smaller than 300 meV/ Å.

(25) WanT code by Ferretti, A.; Bonferroni, B.; Calzolari, A.; Buongiorno Nardelli, M. available at www.wannier-transport.org. See also. Calzolari, A.; Marzari, N.; Souza, I.; Buongiorno Nardelli, M. *Phys. Rev. B* **2004**, *69*, 035108.

(26) (a) Wilmouth, R. C.; Turnbull, J. J.; Welford, R. W. D.; Clifton, I. J.; Prescott, A. G.; Schofield, C. J. *Structure* **2002**, *10*, 93. (b) Unno, H.; Ichimaida, F.; Suzuki, H.; Takahashi, S.; Tanaka, Y.; Saito, A.; Nishino, T.; Kusunoki, M.; Nakayama, T. *J. Biol. Chem.* **2007**, *282*, 15812.

(27) We checked a posteriori the accuracy of the results and their independence from the choice of the basis set. We calculate the electronic structures of cyanidin-3-glucoside in the optimized AH^+, A, A^-, B, C configurations by using a localized atom-centered numeric basis set, as implemented in the Dmol3 code (Delley, B. J. *Comput. Mater. Sci.* **2000**, *17*, 122.) and obtaining the same results. Further tests within local spin density approximation where the spin degrees of freedom are explicitly taken into account converge to the same spin-unconstricted results.

(28) (a) Runge, E.; Gross, E. K. U. *Phys. Rev. Lett.* **1984**, *52*, 997. (b) *Time-Dependent Density Functional Theory*; Marques, M. A. L., Ullrich, C., Nogueira, F., Rubio, A., Burke, K., Gross, E. K. U., Eds; Springer: Berlin, 2006.

(29) Castro, A.; Appel, H.; Oliveira, M.; Rozzi, C. A.; Andrade, X.; Lorenzen, F.; Marques, M. A. L.; Gross, E. K. U.; Rubio, A. *Phys. Status Solidi B* **2006**, *243*, 2465 available at www.tddft.org/programs/octopus.

(30) Norm-conserving pseudopotentials (Troullier, N.; Martins, J. L. *Phys. Rev. B* **1991**, *43*, 1993) are adopted to describe electron-ion interaction, and the adiabatic PBE parameterization for the exchange and correlation potential was employed during the time evolution. The wave functions in the real space were represented by using a uniform grid made of overlapping spheres with a radius of 5 Å centered around each nucleus with a grid spacing of 0.18 Å. For the integration of the time-dependent Kohn−Sham equations, we used a time step of 0.007 fs which assures the stability of the time propagation. A total propagation time of 12 fs results in a resolution of about 0.1 eV in the computed spectrum.

(31) (a) Varsano, D.; Di Felice, R.; Marques, M. A. L.; Rubio, A. *J. Phys. Chem. B* **2006**, *110*, 7129. (b) Marques, M. A. L.; Lopez, X.; Varsano, D.; Castro, A.; Rubio, A. *Phys. Rev. Lett.* **2003**, *90*, 258101. (c) Lopez, X.; Marques, M. A. L.; Castro, A.; Rubio, A. *J. Am. Chem. Soc.* **2005**, *127*, 12329. (d) Castro, A.; Marques, M. A. L.; Alonso, J. A.; Rubio, A. *J. Comput. Theor. Nanosci.* **2004**, *1*, 231.

JP904966D